THE BELL SYSTEM
TECHNICAL JOURNAL

VOLUME XLIV FEBRUARY 1965 NUMBER 2

Numerical Evaluation of Electron Image Phase Contrast

By R. D. HEIDENREICH and R. W. HAMMING

(Manuscript received April 17, 1964)

This paper is concerned with phase contrast in electron images with emphasis on a periodic scattering object. The Kirchoff diffraction or imaging integral over the back focal plane is formulated in terms of the amplitude and phases of the scattered wave, using coordinates adapted to numerical methods. The integral was programmed for evaluation on the IBM 7090 and the image plane amplitude displayed on a microfilm plotter. The effects of spherical aberration, aperture size, defocus and thermal motion of the scattering atoms on image contrast of atom positions for chains of nickel and of gold atoms were investigated for separations of 2 Å and 8 Å.

In the range of atomic separations, spherical aberration is the most destructive single factor in the loss of phase contrast. It appears that an objective lens with a spherical aberration coefficient less than 0.2 mm will be necessary if phase contrast images of atom locations are to be attained. In addition, a practical quarter-wave phase plate is essential for the objective lens system and will be much more effective than defocus contrast. Even so the contrast is marginal for photographic recording except for the case of a thin perfect crystal. Amplitude contrast is very small for atom positions and should be minimized by the use of a large objective aperture.

Phase contrast should improve with increasing accelerating potentials due to reduced inelastic cross sections compensating the loss in elastic contrast near 2×10^5 *volts.*

I. INTRODUCTION

The resolving power and general quality of electron microscope images are determined basically by image plane contrast. There are two distinct contrast mechanisms:

(1) *amplitude contrast* — produced by removal from the image plane of electrons scattered *outside* the objective half-angle, β_{obj}

(2) *phase contrast* — produced by suitable recombination at the image plane of waves scattered within the objective aperture.

The first mechanism, amplitude contrast, is the one commonly operating in images of objects which are greater than about 10 Å in size. The contrast between two image points for this type of object is either *mass thickness* or *diffraction* and is given approximately by

$$\Delta I/I = \Delta(Qt) = Q\Delta t \quad \text{or} \quad t\Delta Q. \tag{1a}$$

for amorphous materials. (See Ref. 1, Ch. IX, for diffraction contrast.) Here Q is the cross section for scattering outside the objective aperture and t is the object thickness. In turn, the cross section for scattering outside the aperture is

$$Q = \frac{N_0 \sigma_{atom}}{A} \rho \tag{1b}$$

with $N_0 = 6.02 \times 10^{23}$ being Avogadro's number. Here, A is the atomic weight and ρ the density. The cross section per atom for scattering outside the aperture is σ_{atom} and consists of an elastic and an inelastic part

$$\sigma_{atom} = \sigma_{el} + \sigma_{incl}. \tag{1c}$$

The cross section σ_{atom} is the fraction of incident electrons scattered beyond the objective half-angle, β_{obj}, and is the integral of the differential cross section, $D(\beta)$, over the scattering angle β

$$\sigma_{atom} = 2\pi \int_{\beta_{obj}}^{\pi} D(\beta) \sin \beta \, d\beta. \tag{1d}$$

The differential cross section, $D(\beta)$, determines the intensity distribution at the back focal plane of the objective lens. For elastic scattering by an isolated atom $D(\beta)$ is simply the square of the atomic scattering amplitude or

$$D(\beta) = |f(s)|^2 \tag{2a}$$

where $f(s)$ is the electron scattering amplitude per atom as a function of the scattering parameter

$$s \equiv 4\pi \frac{\sin(\beta/2)}{\lambda} \tag{2b}$$

with β the scattering angle and λ the incident electron wavelength. For the small scattering angles encountered with fast electrons, $\sin(\beta/2) \approx \beta/2$ and

$$s \approx 4\pi \frac{\beta}{2\lambda}. \tag{2c}$$

Tables of scattering amplitudes [Ref. 2, Tables 3.3.3 A(1) and A(2)] list values of $f(s)$ in Å or cm for chosen values of the parameter $\beta/2\lambda$.

The differential cross section for a solid object is determined by interference among the waves scattered by the individual atoms composing the object. This, in turn, depends upon the spatial arrangement of the atoms. The differential cross section for a liquid or glass is diffuse, with broad maxima corresponding to those interatomic distances occurring most frequently. On the other hand, that for a single crystal is a discrete set of spots.

The portion of the scattered amplitude distribution falling outside the objective aperture determines the amplitude contrast of an image point as sketched in Fig. 1. That part of the distribution falling within the aperture is available for phase contrast at the image plane. The extent to which the phase information can be used in the formation of an image is presently limited by spherical aberration which essentially "scrambles" the phases to a degree increasing as the fourth power of the scattering angle. Phase information concerning the distance between two object points is thus increasingly garbled as the distance between the points decreases. This follows since the scattering angle for a distance a in the object is

$$\beta \approx \lambda/a. \tag{2d}$$

Only values of a such that $\beta < \beta_{\text{obj}}$ have any possibility of contributing to phase contrast.

Although numerical calculation of phase contrast is the purpose of this paper, it is instructive to consider the limitations on amplitude contrast in the region of interatomic separations before discarding it.

II. AMPLITUDE CONTRAST

The total amplitude contrast for a single atom in the object plane of a perfect lens would be

$$\frac{\Delta I}{I_0} \approx -\frac{\sigma_{\text{el}}}{\pi\langle R_{\text{el}}^2\rangle} - \frac{\sigma_{\text{inel}}}{\pi\langle R_{\text{ex}}^2\rangle} \tag{3a}$$

where R_{el} is the scattering radius for elastic collisions and R_{ex} that for

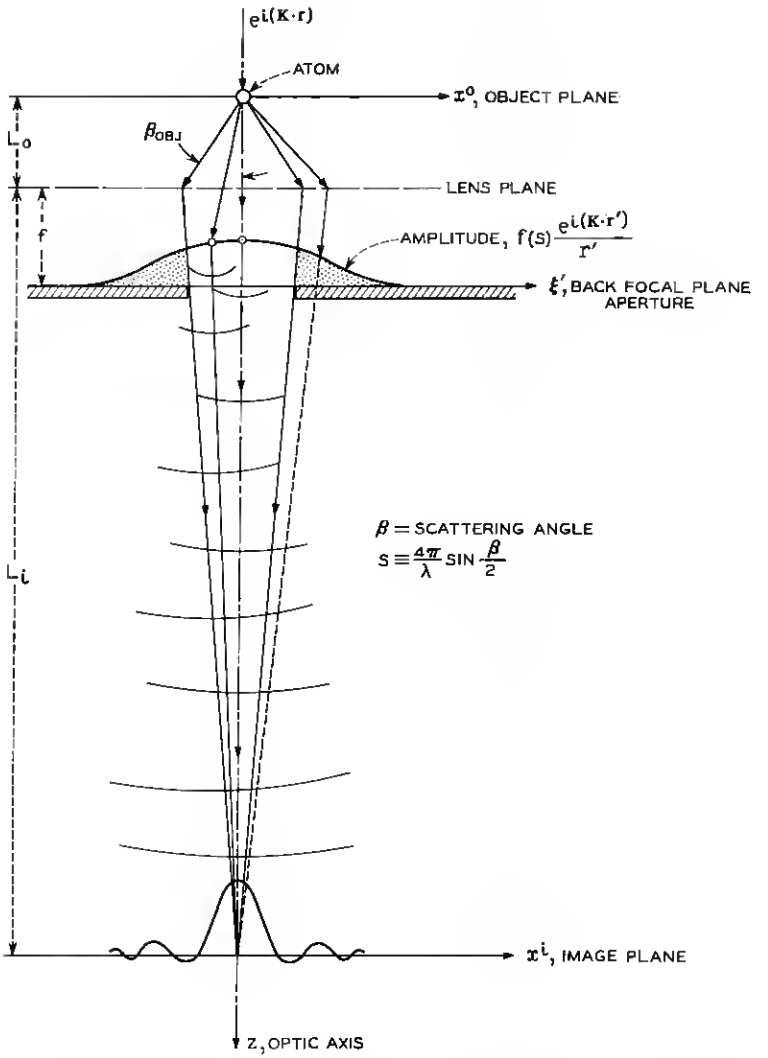

Fig. 1 — Schematic diagram showing amplitude scattered by single atom in object plane. The diffracted amplitude at the back focal plane produces image plane contrast depending upon the size of the aperture. The portion (shaded) falling outside the aperture results in deficiency amplitude contrast. The portion within the aperture can produce phase contrast.

inelastic. If the resolving power of an imperfect objective lens is δ, then $R_{el} \approx \delta$ in (3a). Both terms of (3a) rapidly diminish with increasing incident electron velocity and fixed aperture. The negative sign denotes deficiency contrast for an image point.

Since the scattering contracts into the forward direction as the electron velocity increases, it is advisable to consider the scattering amplitude at constant values of $\beta_{obj}/2\lambda$ (the scattering parameter). This amounts to shrinking the objective aperture as the wavelength decreases so that the Airy diffraction disc from the aperture maintains a constant radius. This is accomplished by changing the variable of integration in (1d) from β to the scattering parameter s of (2b). The elastic cross section for scattering outside the objective aperture (per atom) becomes

$$\sigma_{el} = \frac{\lambda^2(1 - \gamma^2)^{-1}}{2\pi} \int_{(2\pi/\lambda)\beta_{obj}}^{4\pi/\lambda} |f^0(s)|^2 s \, ds \tag{3b}$$

with $\gamma \equiv v/c$, the ratio of electron velocity to that of light. Here $f^0(s)$ is the scattering amplitude based on the electron rest mass. It is noted that the velocity dependence of (3b) results in a rapidly decreasing value of σ_{el} as the accelerating voltage increases, with consequent loss of elastic amplitude contrast in (3a). The elastic cross sections as a function of atomic number have recently been calculated by Burge[3] and Smith using numerical methods with (3b).

The second term of (3a) depends upon the inelastic cross section σ_{inel} and the inelastic excitation radius, R_{ex}. Williams[4] arrived at an excitation distance R_{ex} for an atom of average excitation energy $\langle \Delta E \rangle$ having a velocity dependence

$$R_{ex} \approx \frac{0.2vh}{\langle \Delta E \rangle} (1 - \gamma^2)^{-\frac{1}{2}}. \tag{4}$$

For carbon, R_{ex} is about 40 Å at $V_a = 10^5$ volts taking $\langle \Delta E \rangle \approx 44$ volts, so that the location of the energy loss event is very diffuse. For heavier atoms, R_{ex} is generally less, being about 4 Å for Al at 10^5 volts with $\langle \Delta E \rangle \approx 300$ volts. The inelastically scattered electrons thus do not carry localized information on atom locations (unless they are subsequently diffracted). The relatively large values of R_{ex} make the amplitude contrast due to inelastic scattering trivial except for relatively large objects (50–100 Å).

The amplitude contrast resulting from elastic scattering is so small as to offer little hope of imaging single atoms. For example, the elastic cross section for a nickel atom is about 7×10^{18} cm^2 at $V_a = 5 \times 10^4$ volts

for an objective aperture $\beta_{obj} \approx 5 \times 10^{-3}$ rad. The contrast is only about 0.8 per cent for $\delta \approx 2$ Å, or so low as to be of little importance. The chief hope for imaging atoms with the electron microscope lies in phase contrast, wherein intensities are very sensitive to the relative phases of the scattered waves reconstituted at the image plane.

III. PHASE CONTRAST[1]

The dominant contrast mechanism for scattering objects exhibiting a periodic structure or with a detail size approaching atomic dimensions is that of phase contrast. This requires that the image plane amplitude be evaluated by superposition of all the waves which are scattered by the object and enter the objective aperture of the lens. In its most general form this superposition is the imaging integral.[5] For a perfect, aberration-free objective lens the imaging integral is the Fourier transform of the diffracted amplitude distribution at the back focal plane, which is itself the Fourier transform of the distribution of scattering potential in the object. The imaging integral is thus a magnified representation of the Fourier projection in the object plane of the electrostatic potential distribution[6] in the object itself. In the case of a real objective lens, the fidelity of the image plane amplitude distribution is determined by the lens aberrations and by the size of the objective aperture. The objective aperture limits the distance information available to the image plane, removing the higher "spatial frequencies" in the diffraction pattern at the back focal plane. This is in addition to its own diffraction pattern.

A description of the intensity distribution in the image plane involves a consideration of three planes in the objective lens. These are: (1) the object plane with rectangular coordinates, the x^o-y^o plane, (2) the back focal plane or ξ'-η' plane containing the objective aperture and (3) the image or x^i-y^i plane. The three planes are normal to the optic axis z as shown in Fig. 2. The object and image distances measured from the lens plane are L_0 and L_i respectively. The distance from the lens plane to the back focal plane is the focal length of the lens f. The magnification of the image is $M = L_i/L_0$, and $f \approx L_0$ when $L_i \gg L_0$.

Assume a plane parallel electron beam of wave vector $\mathbf{K}$ along the optic axis incident on the object plane from above. Let its amplitude be unity. Electron waves scattered by the object in the object plane produce a diffraction or scattering pattern at the back focal plane. This pattern is nearly a plane section through the reciprocal lattice of the object with a scale factor $L_0\lambda$, where λ is the electron wavelength and $|\mathbf{K}| = 2\pi/\lambda$. The diffracted amplitude distribution ψ in the back focal plane is in turn a source for Huygens wavelets which propagate to the

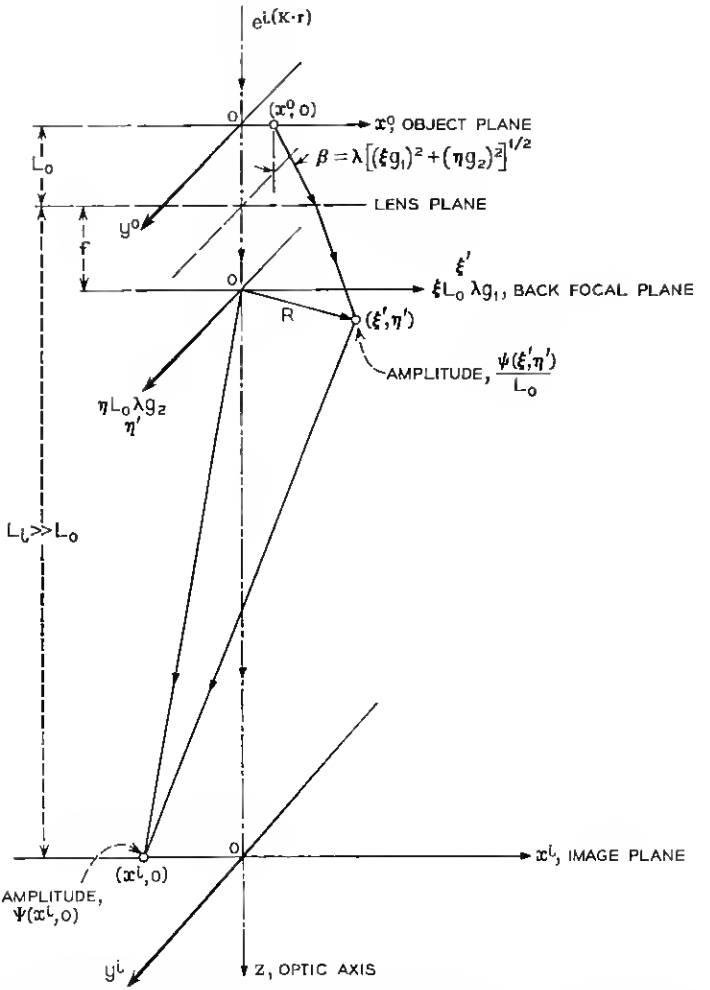

Fig. 2 — The three planes — object, back focal and image — that are of concern in contrast calculations. The scale in the back focal plane is for a periodic scattering object with reciprocal lattice vectors g_1 and g_2.

image plane and recombine according to their phases and so produce the image amplitude distribution. The entire process can be formally described in terms of Fourier transforms, as already mentioned. However, when lens aberrations are present the imaging integral describing the image plane amplitude distribution for the imperfect image is no longer identical with the object plane Fourier projection of potential in the object. It is usually necessary to employ numerical methods in evaluating

the image plane amplitude, since the integration cannot in general be carried out in analytic form. The integral to be considered[7] is

$$\Psi(x^i, y^i) = \frac{1}{L_0 L_i \lambda} \int_{\xi'} \int_{\eta'} \psi(\xi', \eta') \exp [i\chi(\xi', \eta')] \cdot \exp [-iK(\xi' x^i + \eta' y^i)/L_i] \, d\xi' \, d\eta'. \tag{5}$$

$\chi(\xi', \eta')$ is the phase of the amplitude at (ξ', η') in the back focal plane.

Since the primary concern is with crystalline or periodic scattering objects, the coordinate system chosen in the back focal plane is adapted both to this situation and to a formulation lending itself to numerical evaluation. Distances R in the back focal plane are related to distances d in the object by the relation $| R | = L_0\lambda/d$. $L_0\lambda$ is the camera constant or scale factor. A single-crystal object produces an array of diffraction spots in the back focal plane located at $\mathbf{R} = L_0\lambda \mathbf{g}_1 + L_0\lambda \mathbf{g}_2$ where $\mathbf{g}_1$ and $\mathbf{g}_2$ are the operating reciprocal vectors in the object plane. The generating vectors in the object are $\mathbf{a}_1, \mathbf{a}_2, \mathbf{a}_3$ and the generating vectors in reciprocal space are $\mathbf{b}_1, \mathbf{b}_2, \mathbf{b}_3$, subject to the condition

$$\begin{aligned} (\mathbf{a}_i \cdot \mathbf{b}_j) &= \delta_{ij} \\ &= 0 \quad \text{if} \quad i \neq j \\ &= 1 \quad \text{if} \quad i = j \end{aligned} \tag{6a}$$

so that $| \mathbf{b}_1 | = | \mathbf{a}_1 |^{-1}$ etc. and

$$\mathbf{g} = h\mathbf{b}_1 + k\mathbf{b}_2 + l\mathbf{b}_3 \tag{6b}$$

where h,k,l are the Miller indices denoting the reciprocal lattice vector $\mathbf{g}$.

Let ξ and η be numbers such that an arbitrary point in the back focal plane is the terminus of the vector $\mathbf{R}$

$$\mathbf{R}(\xi', \eta') = \xi L_0\lambda \mathbf{g}_1 + \eta L_0\lambda \mathbf{g}_2 . \tag{6c}$$

If ξ and η are integers, R locates a diffraction spot at a distance

$$| R | = [(\xi L_0\lambda g_1)^2 + (\eta L_0\lambda g_2)^2]^{\frac{1}{2}} \tag{6d}$$

since the ξ and η axes are rectangular. The scattering angle β for electrons to the point $\mathbf{R}$ is, for small angles ($\sin \beta \approx \beta$)

$$\beta = \frac{| R |}{L_0} = \lambda[(\xi g_1)^2 + (\eta g_2)^2]^{\frac{1}{2}} \tag{6e}$$

and the scattering parameter s is

$$s \equiv \frac{4\pi}{\lambda} \sin \frac{\beta}{2} \approx 2\pi[(\xi g_1)^2 + (\eta g_2)^2]^{\frac{1}{2}}. \tag{6f}$$

The amplitude at a point (x^i, y^i) in the image plane is the diffraction integral[8] over the aperture

$$\begin{aligned}\Psi(x^i, y^i) &= \frac{1}{L_0 L_i \lambda} \int_{-\max}^{+\max} \int \psi(\mathbf{R}) e^{i\chi(\mathbf{R})} \\ &\quad \cdot \exp\left[-2\pi i(\xi x^0 g_1 + \eta y^0 g_2)\right] d(L_0\lambda\xi g_1) d(L_0\lambda\eta g_2) \\ &= \frac{(L_0\lambda)^2 g_1 g_2}{L_0 L_i \lambda} \int_{-\xi_{\max}}^{\xi_{\max}} \int_{-\eta_{\max}}^{\eta_{\max}} \psi(\xi,\eta) e^{i\chi(\xi,\eta)} \\ &\quad \cdot \exp\left[-2\pi i(\xi x^0 g_1 + \eta y^0 g_2)\right] d\xi\, d\eta. \end{aligned} \tag{7a}$$

In order to evaluate (7a) it is necessary to know the amplitude distribution $\psi(\xi, \eta)$ and the phase $\chi(\xi, \eta)$ in the back focal plane.

If the diffraction pattern has a center of symmetry at the origin of the back focal plane, the periodic object likewise has a center of symmetry at the origin of the object plane. In this case the imaging integral (7a) can be simplified for the purposes of calculation to

$$\begin{aligned}\Psi(x^i, y^i) &= \frac{2\lambda g_1 g_2}{M} \int_0^{\xi_{\max}} \int_0^{\eta_{\max}} \psi(\xi,\eta)[\cos\chi(\xi,\eta) + i \sin\chi(\xi,\eta)] \\ &\quad \times \cos 2\pi\xi x^0 g_1 \cos 2\pi\eta y^0 g_2 d\xi\, d\eta. \\ &= \frac{2\lambda g_1 g_2}{M} S^i \end{aligned} \tag{7b}$$

where S^i denotes the phase integral in (7b).

It is now necessary to choose expressions for the amplitude $\psi(\xi, \eta)$ at the back focal plane occurring in (7b). This amplitude depends upon the detailed spatial arrangement of atoms in the object plane and upon the atomic scattering amplitude $f(s)$. There are two approaches to $\psi(\xi, \eta)$ — the kinematic and the dynamical theories of electron diffraction.[9]

The kinematic approach is much the simpler of the two and will illustrate the pertinent features in phase contrast. Since the main interest here is with scattering objects which are basically periodic, the kinematic amplitudes at the back focal plane can be immediately written down. Let the object be a crystal sheet with an atom at the origin of coordinates in the object plane. If the lateral extent of the crystal is n_1 atoms along x^0 and n_2 atoms along y^0 and if the extent in the z direction is n_3 atoms, the kinematic amplitude is the familiar expression[10]

$$\psi(\xi,\eta) = (1 - \gamma^2)^{-\frac{1}{4}} f^0(s) n_3 \frac{\sin \pi n_1 \xi}{\sin \pi\xi} \cdot \frac{\sin \pi n_2 \eta}{\sin \pi\eta} \tag{8}$$

where n_1, n_2, and n_3 are odd integers. If even integers are employed, phase factors must be included in (8). The discussion is therefore confined to odd values. The atomic scattering amplitude $f^0(s)$ is based on the rest mass of the electron and $(1 - \gamma^2)^{-\frac{1}{2}}$ is the relativistic correction (with γ the ratio of electron velocity to that of light). It is noted that

$$\pi n_1 \xi = \frac{|K|}{2} n_1 \frac{\beta_1}{g_1}$$

and

$$\pi n_2 \eta = \frac{|K|}{2} n_2 \frac{\beta_2}{g_2}.$$

The phase χ in the back focal plane is made up of several terms[11]

$$\chi(\xi,\eta) \equiv \frac{\pi}{2} - \frac{2\pi}{\lambda} C_5 \beta^4 + \frac{\pi}{\lambda} \pi \Delta f \beta^2. \tag{9a}$$

The phase change upon diffraction by the object is $\pi/2$, while the second term is the phase due to spherical aberration. The third term is the phase introduced by defocusing the lens an amount Δf. There is a fourth term which is the phase associated with the electron scattering amplitude $f(s)$ for an atom, but it is small except for the heaviest atoms and at large scattering angles and will be neglected here.

It should be mentioned that the spherical aberration phase term in (9a) is four times larger than that commonly used in discussions[12,13] of the effect of spherical aberration. The term in (9a) applies to a *single* ray at angle β with a corresponding circle of aberration of radius $C_5\beta^3$. The unweighted *average* radius for a bundle of rays filling the range $0 < \beta < \beta_{\max}$ is

$$\langle \Delta x^0 \rangle_{sp} = \frac{C_5}{\beta_{\max}} \int_0^{\beta_{\max}} \beta^3 d\beta = \frac{1}{4} C_5 \beta_{\max}{}^3$$

with a resultant average phase

$$\langle \chi \rangle_{sp} = \frac{2\pi}{\lambda} \frac{C_5 \beta_{\max}{}^3}{4}. \tag{9b}$$

The use of (9b) in (9a) in evaluating the imaging integral is not correct, since it suppresses the destructive effect of spherical aberration.

The total amplitude at an image point is the sum of the scattered amplitude (7b) and the unscattered axial wave. If the incident amplitude is unity, then in the kinematic approximation of weak scattering the unscattered wave leaving the object plane is very nearly of unit ampli-

tude. Its amplitude at the origin of the back focal plane is large, but at the image plane it is $(M)^{-1}$. Adding the unscattered amplitude to (7b) yields the total image point amplitude

$$\Psi(x^i, y^i)_{\text{total}} = \frac{1}{M}\left[1 + 2\lambda g_1 g_2 (1 - \gamma^2)^{-\frac{1}{2}} S^i\right]. \tag{10a}$$

The mass correction factor $(1 - \gamma^2)^{-\frac{1}{2}}$ has been removed from S^i so that the velocity dependence of the amplitude can be easily seen. The expression (10a) does not apply when dynamical conditions[14] are realized in the object, since then the axial wave may be weaker than the scattered amplitude and the approximation is no longer valid.

The image point intensity obtained by multiplying (10a) by its complex conjugate is

$$|\Psi(x^i, g^i)|^2 \approx \frac{1}{M^2}\left[1 + 4\lambda g_1 g_2 (1 - \gamma^2)^{-\frac{1}{2}} S^i{}_{\text{real}}\right] \tag{10b}$$

since the term in $|S^i|^2$ will generally be trivial compared to the cross product term until the mass correction term becomes large at very high accelerating voltages ($\approx 10^6$ volts). The imaginary part of the scattered amplitude (7b) is here neglected.

The kinematic contrast G between two image points is defined to be the intensity difference between the respective points divided by the background intensity. Using (10b) the result is

$$G \approx 4\lambda g_1 g_2 (1 - \gamma^2)^{-\frac{1}{2}} \Delta S^i \tag{10c}$$

with all lengths in angstroms. ΔS^i is the amplitude differential between the image points in question obtained by numerical evaluation of

$$S^i = n_3 \int_0^{\xi_{\max}} \int_0^{\eta_{\max}} f^0(s) \frac{\sin n_1 \pi \xi}{\sin \pi \xi} \frac{\sin n_2 \pi \eta}{\sin \pi \eta} \times \cos \chi(\xi,\eta) \cos 2\pi \xi x^0 g_1 \cos 2\pi \eta y^0 g_2 \, d\xi \, d\eta \tag{10d}$$

at each point.

For the purpose of phase contrast calculations it is sufficient to consider a single chain of atoms of spacing a lying along the x^0 axis. The number of atoms in the chain is n_1, with the middle atom on the optic axis. Setting $n_2 = n_3 = 1$ in (10d) gives the integral to be evaluated at a point on the x^i axis as

$$S^i = \int_0^{\xi_{\max}} \int_0^{\eta_{\max}} f^0(s) \frac{\sin \pi n_1 \xi}{\sin \pi \xi} \cos \chi(\xi,\eta) \cos 2\pi \left(\frac{x^0}{a}\right) \xi \, d\xi \, d\eta \tag{10e}$$

having maxima at the image points corresponding to atoms or where $x^0 = 0, \pm a, \pm 2a, \cdots$ etc. The amplitude maxima for atomic positions approach

$$\int_0^{\xi_{\max}} \int_0^{\eta_{\max}} f^0(s) \frac{\sin \pi n_1 \xi}{\sin \pi \xi} \cos \chi(\xi,\eta) d\xi \, d\eta \to \int_0^{\infty} \int_0^{\infty} f^0(s) \cos \chi(\xi,\eta) d\xi \, d\eta$$

as the size of the objective aperture, $\xi_{\max}$, $\eta_{\max}$, increases. The value of the maxima is seen to be sensitive to the phase $\chi(\xi, \eta)$. For a perfect lens, the scattered amplitude in the Gaussian image plane vanishes, since $\chi \approx \pi/2$, so there will be only background intensity. On the other hand, the introduction of a quarter-wave phase plate[15] into the scattered beams can make $\chi = 0$ or π and the amplitude will be a maximum. The sign of the maxima will be that of cos χ, so that atom positions can be either bright or dark against the background, depending upon the phase.

IV. NUMERICAL RESULTS

4.1 *Spherical Aberration at the Gaussian Image Plane*

Numerical evaluation of the phase integral S^i in (7b) requires that the phase (9a) be expressed in terms of the dimensionless coordinates (ξ, η) using (6e) to give

$$\chi(\xi, \eta) = (\pi/2) - 2\pi C_5 \lambda^3 [(\xi g_1)^2 + (\eta g_2)^2]^2 + \pi \Delta f \lambda [(\xi g_1)^2 + (\eta g_2)^2].$$

For the single-atom chain of spacing a this reduces to

$$\chi(\xi, \eta) \approx (\pi/2) - \pi C_5' [\xi^2 + \eta^2]^2 + \pi \Delta f' (\xi^2 + \eta^2) \qquad (11a)$$

with $C_5' = 2C_5\lambda^3/a^4$ and $\Delta f' = \Delta f \lambda / a^2$ being dimensionless aberration and defocus parameters. It is noted that $\frac{1}{2}C_5'$ is the number of wavelengths of spherical aberration at the first diffraction maximum ($\xi = 1$, $\eta = 0$) while $\frac{1}{2}\Delta f'$ is the number of wavelengths of defocus.

In the Gaussian image plane $\Delta f = 0$ and (11a) becomes

$$\chi(\xi, \eta) = (\pi/2) - \pi C_5' [\xi^2 + \eta^2]^2. \qquad (11b)$$

The real phase integral S^i along the chain, $y^0 = 0$, is now

$$S^i = \int_0^{\xi_{\max}} \int_0^{\eta_{\max}} \psi(\xi,\eta) \cos \chi(\xi,\eta) \cos 2\pi \xi x^0/a \, d\xi \, d\eta \qquad (12)$$

and the absolute amplitude is $2\lambda a^{-2} S^i$. If the phase (11b) is used in (12) it is evident that cos χ = sin $\pi C_5' [\xi^2 + \eta^2]^2$. The trivial contrast observed is produced by spherical aberration. Fidelity contrast at the

Gaussian image plane requires the use of a $\lambda/4$ wave plate in the back focal plane. If the plate advances only the diffraction spectra but not the unscattered or zero-order beam, the phase term in (12) is

$$\cos \chi = -\cos \pi C_5' [\xi^2 + \eta^2]^2$$

and the image will display atom positions dark relative to the background.

Since analytical expressions for the atom scattering factors are not available, the amplitude in the back focal plane for this purpose is obtained numerically from tabular values as described in the Appendix. A discussion of the choice of sampling intervals along the ξ, η and x^0/a axes is also found in the Appendix and some of the artifacts that may occur are pointed out.

If $C_5' = 0$ and $n_1 = 1$ in (12), it will be noted that S^i is the profile of the Airy disk[16] for a single atom in the object plane due to diffraction by the objective aperture. Fig. 9(b) of the Appendix shows a computer plot (IBM-7090 microfilm plotter) of (12) for this case of a single nickel atom. The absolute maximum amplitude is 7.7 λ angstrom, or a contrast of about 60 per cent relative to background for 100-kv electrons. The value $a = 2$ Å was employed in (10c), since the scaled $f^0(s)$ curve was at this value of a. The contrast is independent of the number of atoms, n_1, in the chain but is proportional to n_2, the number of atoms along the optic axis if chains are stacked one directly above the other.

Since the electron microscope objective aperture imposes a finite upper bound on the imaging integral the result is equivalent to terminating or truncating a Fourier series to a finite number of terms. As a consequence, the imaging integral does not converge to the value expected for an infinite upper bound but oscillates about this value. The Gibbs phenomenon[17] in the particular case of the objective aperture manifests itself as the experimentally observed diffraction pattern of the aperture. The same phenomenon gives rise to artifacts between atom positions in the image when a finite number of diffraction spectra are admitted by the aperture.[18]

The devastating effect of spherical aberration upon phase contrast in the image of an atom chain is illustrated in the series of amplitude profiles of Fig. 3. The numerical values are for nickel with a spacing of 2Å. Profiles were obtained for chain lengths of 5 and 17 atoms which are within the transverse coherence[19] length of double condenser illumination in present microscopes. Inelastic scattering and thermal motion are neglected. The former is reduced by increasing the accelerating potential and the latter by reducing the temperature. The profiles of Fig. 3 speak

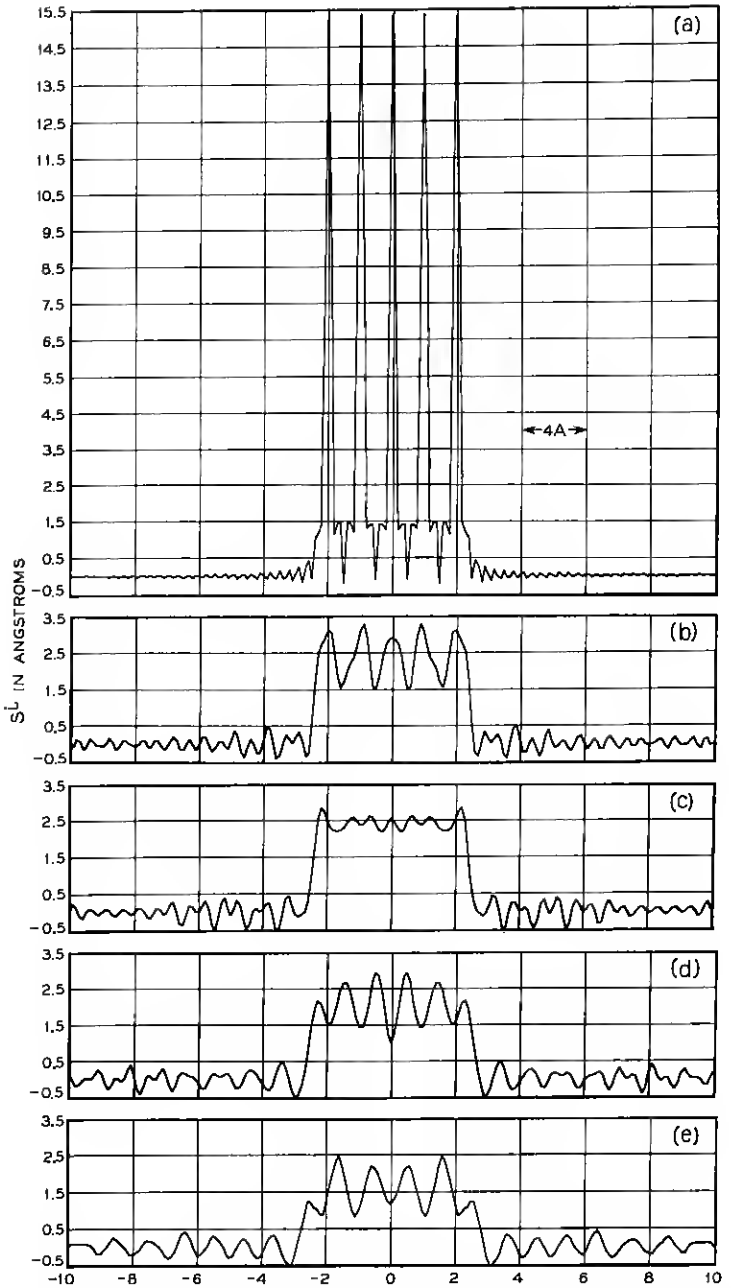

Fig. 3 — Series of numerical image amplitude profiles for a 5-atom chain of nickel atoms with spacing $a = 2$ Å. The effect of increasing spherical aberration parameter C_5' ($\frac{1}{2}\,C_5'$ is the number of wavelengths of aberration at the first diffraction maximum) is illustrated in the series (a)–(e): (a) $C_5' = 0$, (b) 0.2, (c) 0.3, (d) 0.5, and (e) 1.0. A quarter-wave phase plate is assumed present in the back focal plane. The contrast of about 60 per cent in (a) falls rapidly to about 9 per cent in (b) for 100-kv electrons with $f = 3$ mm.

for themselves, showing a loss in atom position amplitude from 15.5 Å with $C_{\bar{0}}' = 0$ to 2 Å with the introduction of 0.1 wavelength of spherical aberration at the first diffraction maximum where $C_{\bar{0}}' = 0.2$.

If the diffraction spectra in the back focal plane were points, as for an infinite, perfect crystal, the phase contrast would be periodic with $C_{\bar{0}}'$ and would have maxima where $(\Delta x^0)_{\text{sph}} = C_{\bar{0}}\beta^3$ is an integral number of half-lattice spacings. For the finite chains of 5 and 17 atoms, the damped periodic nature of the contrast is illustrated in Figs. 4(a) and (b) compared to that for a single atom. The aperture has been decreased from 3.5 diffraction maxima in Fig. 4(a) to 1.5 in Fig. 4(b) with a sizable reduction in contrast. The reduction in aperture size further limits the amount of spherical aberration but this is more than compensated for by the loss of distance information in the diffraction pattern and the increased diffraction by the aperture. It must be concluded that if useful phase contrast of atom positions is to be obtained spherical aberration must be minimized. Other contrast enhancing devices cannot overcome this defect of disturbed phase information.

4.2 *Contrast by Defocus with Spherical Aberration*

A case approximating the present state of the electron microscope objective lens is that for no phase plate with $C_{\bar{0}} \approx 3$ mm and contrast enhancement by defocus. This example is a chain of 5 gold atoms with a spacing of 8 Å and was chosen to approximate the situation of gold-stained sites on a DNA molecule.[20] No allowance is made for a substrate or inelastic scattering.

The phase (11a) for this particular case retains $\pi/2$ (with no phase plate) as well as the defocus term. The scaled aberration parameter is now $C_{\bar{0}}' = 0.74$ or 0.37 wavelengths at the first diffraction maximum using 100-kv electrons. A series of amplitude profiles was computed on the IBM 7090 for a range of values $0 \leqq \Delta f' \leqq 4$. From these results the relative amplitude of atom positions ΔS^i was plotted against $\Delta f'$ as shown in Fig. 5. The oscillation of contrast with changing defocus is typical with near zero contrast at exact focus. Maximum contrast is obtained by weakening the objective lens (Δf positive) as is well known. Even so the contrast does not rise above about 6 per cent, which is submarginal for seeing the gold atom positions in the image.

If the spherical aberration coefficient is reduced to 2 mm or $C_{\bar{0}}' \approx 0.5$ with 0.25 wavelengths at the first diffraction maxima, the maximum defocus contrast rises to around 9 per cent for a gold atom with 100-kv electrons. The neglect of substrate, thermal motion and inelastic scattering again renders the visibility of single gold atoms marginal at best.

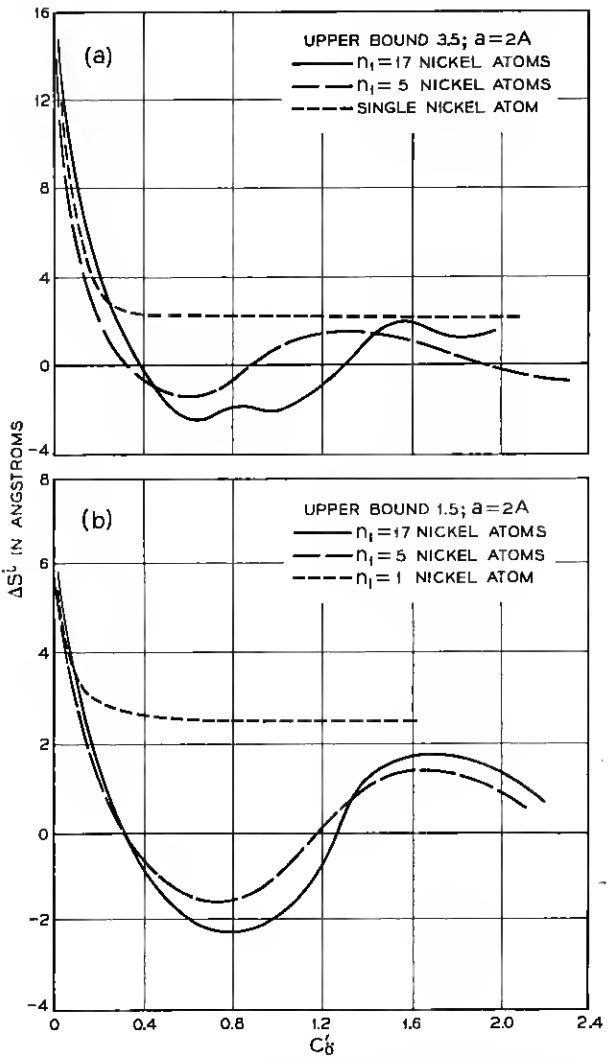

Fig. 4 — Plot of ΔS^i vs $C_5' = 2C_5\lambda^3/a^4$ for nickel atom chains of 5 and 17 atoms. The curves approximate damped, periodic functions. The kinematic contrast is $G = 4.4\ \Delta S^i$ per cent for $f = 3$ mm using 100-kv electrons. The upper bound is 3.5 diffraction maxima in (a) and 1.5 in (b).

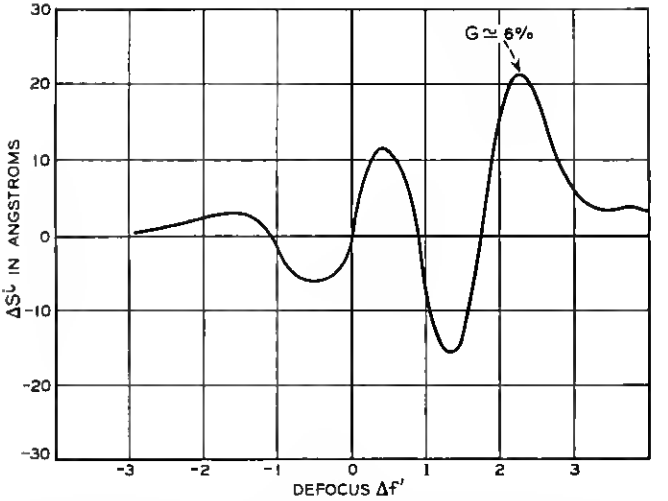

Fig. 5 — Defocus phase contrast for a chain of 5 gold atoms with 8 Å spacing and a spherical aberration parameter $C_5' = 0.74$ or 0.37 wavelengths at the first diffraction maximum ($C_5 = 3$ mm). The defocus is $\frac{1}{2}\Delta f'$ wavelengths or $\Delta f = 1730\ \Delta f'$ angstrom. The contrast is $G \approx 0.28\ \Delta S'$ per cent at 100 kv.

However, a clump of three gold atoms at the staining sites might be visible in the image, since this would multiply the contrast by a factor of roughly two. There might be also some benefit from amplitude contrast providing the phase and amplitude contrast are the *same* sign and that the image points for the two coincide. A small shift in image points by unsymmetric phase would separate the phase and amplitude image points, resulting in confusion.

If the diffraction spectra at the back focal plane are discrete points, the condition for maximum phase contrast by defocus is that the phase (11a) be $n\pi$ where n is an integer. The optimum defocus parameter $\Delta f'$ is then

$$\Delta f' = (n - \tfrac{1}{2}) + C_5'$$

a relation useful in estimating the amount of defocus for best contrast. Because defocus can optimize only one object plane spacing at a time, a phase plate is much to be preferred wherein all spacings are maximized in the same image plane.

4.3 *Effect of Thermal Motion*

The scattering amplitude $\psi(\xi, \eta)$ in (12) assumes that the atoms in the object plane are stationary. This is not true, since they possess ther-

mal motion which is temperature-dependent and zero-point motion at the absolute zero of temperature. Detailed analysis of thermal vibration amplitudes in a solid is a complex problem[21] which need not be discussed here. To a first approximation the effect of an isotropic thermal motion is described by the Debye-Waller factor e^{-M} to produce an effective atom scattering amplitude

$$(1 - \gamma^2)^{-\frac{1}{2}} f^0(s) e^{-M}.$$

This dependence has been recently experimentally verified by Horstmann and Meyer.[22] The uncertainty lies in the evaluation of M. For the isotropic averaged vibration case, M is given by

$$\frac{8\pi^2}{\lambda^2} \langle u^2 \rangle \sin^2 \beta/2 \approx 2\pi^2 \langle u_a^2 \rangle [(\xi g_1)^2 + (\eta g_2)^2]$$

for small angles. For the simple one-dimensional grating $\langle u_a \rangle^2$ is the mean square atom displacement along the chain. The Debye factor is then

$$M \approx 2\pi^2 \frac{\langle u_a^2 \rangle}{a^2} (\xi^2 + \eta^2) \tag{13}$$

and the effect of thermal vibrations on contrast can be approximated by introducing e^{-M} into the phase integral (12). The thermal diffuse amplitude is neglected, as is the inelastic scattering, so that again the computed contrast will be higher than could actually be expected. The effect on contrast of thermal motion alone arising through diminution of the diffracted amplitudes is illustrated using (12) and setting $C_5' = \Delta f' = 0$ and inserting a quarter-wave plate in the back focal plane. Amplitude profiles for a range of values of the relative mean square displacement were computed. The results are summarized in Fig. 6, showing $\Delta S'$ as a function of $\langle u_a^2 \rangle^{\frac{1}{2}}/a$. The contrast for stationary atoms is 60 per cent, as before, but falls to 30 for a relative mean square thermal displacement of 0.1. If spherical aberration were introduced, the contrast of atom positions would rapidly fall below that necessary for visibility in the usual microscope viewing system.

V. DISCUSSION

The foregoing numerical results serve to point up the rather severe requirements for an objective lens system capable of yielding phase contrast images of atoms. The highly destructive influence of spherical aberration is a major hurdle that must be reduced to a minimum. If an objective lens with $C_5 \approx 1$ mm can be realized, the best contrast obtain-

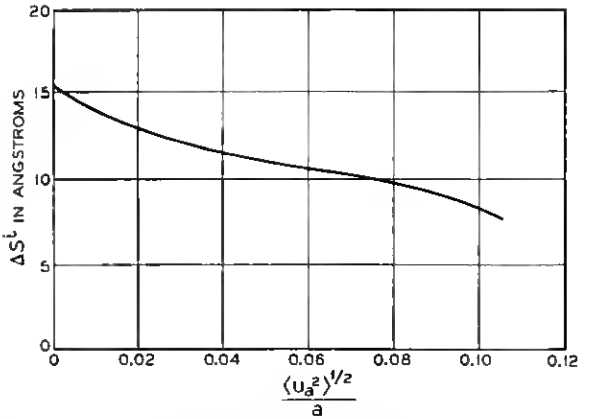

Fig. 6 — Effect of thermal motion on image profile maximum amplitude; $\langle u_a^2 \rangle^{\frac{1}{2}}$ is the root mean square amplitude along the chain. The values are for nickel atoms with $a = 2$ A and $C_5' = \Delta f' = 0$.

able with an ideal phase plate will be around 10 per cent for an individual nickel atom in a chain. The situation is much more favorable for a thin crystal of the order of 50 Å thick, wherein the diffraction spectra are greatly reinforced. For the single layer of atoms it may be necessary to turn to image intensifiers in combination with communication techniques of extracting a useful signal from background noise.

Practical considerations demand ultra-high vacuum to eliminate contamination by electron bombardment. A cryogenic stage will be useful to reduce loss of contrast due thermal motion. The problem of background noise in the image from a substrate can be circumvented either by a self-supporting specimen over a small hole or by using thin single-crystal substrates. The noise level from carbon substrates is intolerably high for this purpose.

The rapid decline of inelastic scattering cross sections with increasing accelerating voltage should offset the reduced elastic contrast predicted by (10c), suggesting that potentials in the range 150–200 kv should be appropriate. This is just opposite to the use of lower electron velocities for amplitude contrast.

It appears necessary to develop a practical quarter-wave contrast plate for the back focal plane. The thickness t of a region of potential V_0 required to introduce a phase advance of $\pi/2$ is[23]

$$\frac{\pi V_0 t}{\lambda V_a} = \frac{\pi}{2} \quad \text{or} \quad t = \frac{\lambda V_a}{2V_0}$$

where V_a is the accelerating voltage. A material film of inner potential

V_0 is a possibility, but the elastic and inelastic scattering by the film itself must be reckoned with.

The authors would like to acknowledge the invaluable aid of Miss Barbara Dale, who programmed the imaging integral and carried out the computational procedures and checks.

APPENDIX

The appropriate numerical values of the amplitude in the back focal plane are obtained from tabular values of the atom scattering factors. The scale factor for $f^0(s)$ in the back focal plane requires that

$$\sqrt{\xi^2 + \eta^2} = 2a \frac{\sin \beta/2}{\lambda} .$$

For a nickel atom chain with $a = 2$Å, the first diffraction maximum is at $(\sin \beta/2)/\lambda = 0.25$ and $\sqrt{\xi^2 + \eta^2} = 1$, for which $f^0 = 3.22$ Å, corresponding to a scattering angle $\beta = \lambda/a \sqrt{\xi^2 + \eta^2} = 1.8 \times 10^{-2}$ rad. The empirical curve $f^0(\sqrt{\xi^2 + \eta^2})$ is obtained from the tabular values using a third-order Lagrange interpolation[24] stored on tape for use in evaluating the integral (12) on the IBM 7090.

The phase integral S' is put into suitable form for machine computation by dividing each of three axes, ξ, η and x/a into equally spaced intervals. The intervals along the three axes are $\overline{\Delta\xi}$, $\overline{\Delta\eta}$, and $\Delta(x/a)$ respectively. A point in the ξ-η plane now becomes a point in a grid with coordinate $(m_1\overline{\Delta\xi}, m_2\overline{\Delta\eta})$, where m_1 and m_2 are integers. The value of the integral (12) is now approximated by a summation over the integers m_1 and m_2

$$\sum_{m_1=0} \sum_{m_2=0} f^0 \left(\sqrt{(m_1\overline{\Delta\xi})^2 + (m_2\overline{\Delta\eta})^2}\right) \frac{\sin \pi n_1 m_1 \overline{\Delta\xi}}{\sin \pi m_1 \overline{\Delta\xi}} \cos 2\pi \left(\frac{x}{a}\right) m_1\overline{\Delta\xi}. \quad (14)$$

The Fourier integral (12) is thus approximated by a Fourier series (14). This raises the question of how well the series converges to the integral, which in turn is determined by the size of the intervals $\overline{\Delta\xi}$ and $\overline{\Delta\eta}$ and by m_1 and m_2. Since a Fourier series is periodic, it not only approximates the integral in the range of the function S' but produces repetitive images outside the range.

The importance of the intervals $\overline{\Delta\xi}$ and $\overline{\Delta\eta}$ in the back focal plane lies in the fact that they set a limit to the information available at the image plane. High fidelity of the image point amplitudes requires that $\overline{\Delta\xi}$ and $\overline{\Delta\eta}$ be as small as possible relative to the amplitude detail in the back focal plane. Along the η axis, the amplitude is a monotonic decreasing

function with gradual changes in slope. Along the ξ axis the situation is quite different, as seen in Fig. 7, where IBM 7090 microfilm plots of the diffraction amplitude or Fourier coefficient in (10d) are shown for $n_1 = 5$ and $n_1 = 17$ atoms. The interval along ξ is $\overline{\Delta\xi} = 0.01$. The half width of the primary maxima is $(\Delta\xi)_{\frac{1}{2}} = 1/n_1$, so that a good approximation first requires that

$$\overline{\Delta\xi} \ll (\Delta\xi)_{\frac{1}{2}} = \frac{1}{n_1}$$

or

$$\overline{\Delta\xi} n_1 \ll 1. \tag{15}$$

Between the principle maxima of spacing unity there are $(n_1 - 2)$ subsidiary maxima and minima. The actual spacing of these subsidiaries is

$$\frac{1 - 2(\Delta\xi)_{\frac{1}{2}}}{n_1 - 2} = \frac{1}{n_1}$$

and at least three points are required to locate a maximum, zero, and then the minimum. If it is arbitrarily assumed that six points are a reasonable sampling density between adjacent maxima and minima, the sampling interval must be

$$\overline{\Delta\xi} \leqq \frac{1}{6n_1}$$

or

$$\overline{\Delta\xi} n_1 \leqq \frac{1}{6}.$$

On this basis, then, $\overline{\Delta\xi} = 0.01$ is adequate for $n_1 = 5$. If $n_1 = 17$, however, then $\overline{\Delta\xi} \leqq 1/102$ or the interval $\overline{\Delta\xi}$ is just adequate. As the number of atoms in the chain increases further the detail in the amplitude distribution soon becomes smaller than $\overline{\Delta\xi} = 0.01$. The interval $\overline{\Delta\xi} = 0.01$ is thus considered too crude for $n_1 > 25$ atoms. This is admittedly rather arbitrary, and a more detailed analysis might discover a better criterion.

Along the η axis, on the other hand, an interval $\overline{\Delta\eta} = 0.1$ is quite adequate and reduces the number of sampling points. Under these conditions the number of sample points in the back focal plane for each image point is

$$\frac{\eta_{\max}}{\Delta\eta}\frac{\xi_{\max}}{\eta\xi} = 12.7 \times 10^3; \qquad \xi_{\max} = \eta_{\max} = 3.5. \tag{16}$$

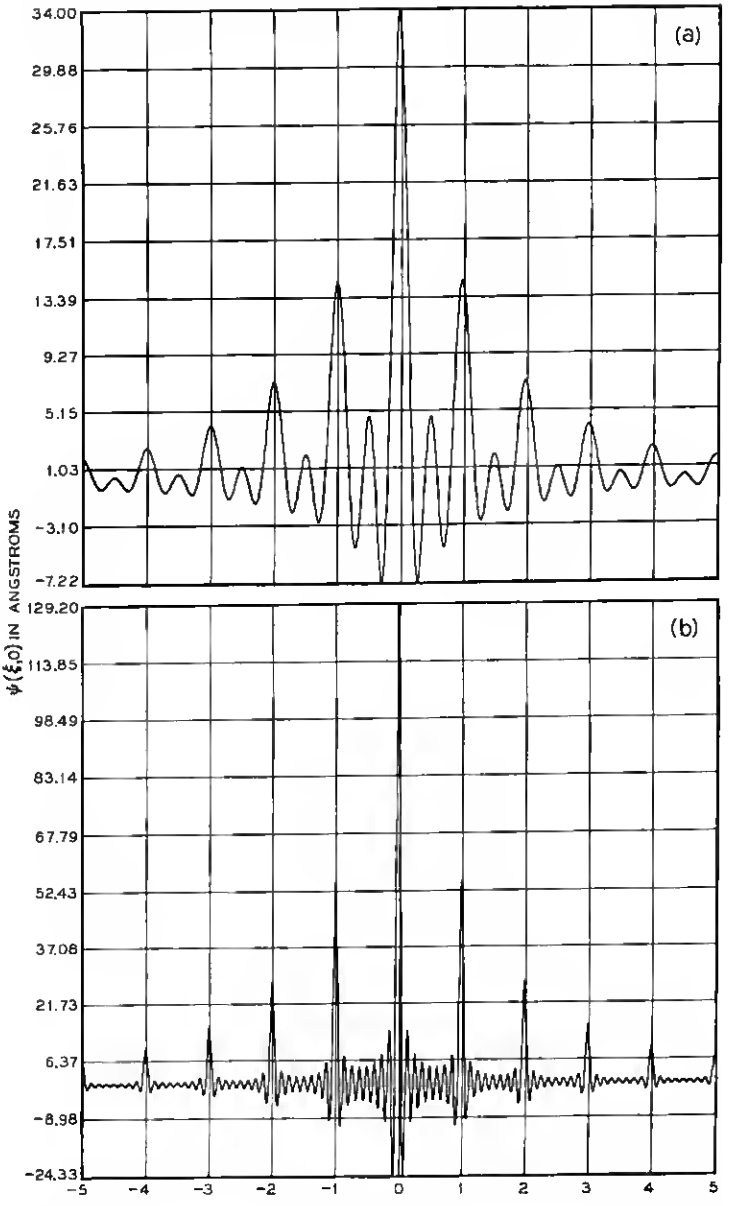

Fig. 7 — Diffracted amplitude distributions at the back focal plane as obtained from the microfilm tracer on the IBM 7090 for a sampling interval $\Delta\xi = 0.01$; the grating spacing is $a = 2$ Å: (a) for a chain of 5 nickel atoms; (b) for a chain of 17 nickel atoms.

The remaining consideration relating to the sample intervals is *aliasing*. This behavior can be illustrated by returning to (14). Writing the coefficient as $\phi(\xi, \eta)$, the series sums at $(x/a) = 0$ to

$$S_{\text{real}}{}^{i}(0) = \sum_{m_1=0} \sum_{m_2=0} \phi(\xi,\eta). \tag{17a}$$

If the sampling interval along x is $\Delta(x/a)$, then the sum at an image point $x = j\Delta(x/a)$ with j an integer is

$$S_{\text{real}}{}^{i}\left(j\Delta\left(\frac{x}{a}\right)\right) = \sum_{m_1=0} \sum_{m_2=0} \phi(\xi,\eta) \cos 2\pi j\Delta\left(\frac{x}{a}\right) m_1\overline{\Delta\xi}. \tag{17b}$$

If $2\pi j\Delta(x/a)m_1\overline{\Delta\xi}$ = multiple of 2π then the cosine terms are unity and (17a) and (17b) are equal. Thus

$$j\Delta\left(\frac{x}{a}\right)\overline{\Delta\xi} = \text{integer}. \tag{17c}$$

The *aliasing period*[25] is then

$$\Delta j = \frac{1}{\Delta\left(\frac{x}{a}\right)\overline{\Delta\xi}}$$

or

$$\text{alias period} = \frac{1}{\overline{\Delta\xi}}. \tag{17d}$$

Thus the critical sampling interval for these computations is $\overline{\Delta\xi}$, since it determines both the resolution (15) and the aliasing period. The effect is well illustrated in Fig. 8, comparing the profiles for $n_1 = 5$ with $\overline{\Delta\xi} = 0.01$ and $\overline{\Delta\xi} = 0.1$. The repeating nature of the image or aliasing is evident for $\overline{\Delta\xi} = 0.1$ when the aliasing period is only ten. With $\overline{\Delta\xi} = 0.01$, the period is 100 and not seen on the plot. If the number of atoms n_1 were now increased to nine the image profile with $\overline{\Delta\xi} = 0.1$ would show no break at the end of an atom chain and so would appear to be an infinite chain.

The sampling interval along the x^i axis in the image plane has an effect on the representation of the finer details in the profile. When the detail approaches the interval length $\Delta(x/a)$ the representation becomes inaccurate with "bumps" and "angles" rather than a smooth curve. This is illustrated in Fig. 9 for the case of a single atom, $n_1 = 1$, for which

$$S^i\left(j\Delta\left(\frac{x}{a}\right)\right) = \sum_{m_1=0} \sum_{m_2=0} f\left(\sqrt{(m_1\overline{\Delta\xi})^2 + (m_2\overline{\Delta\eta})^2}\right) \cos 2\pi j\Delta\left(\frac{x}{a}\right) m_1\overline{\Delta\xi}$$

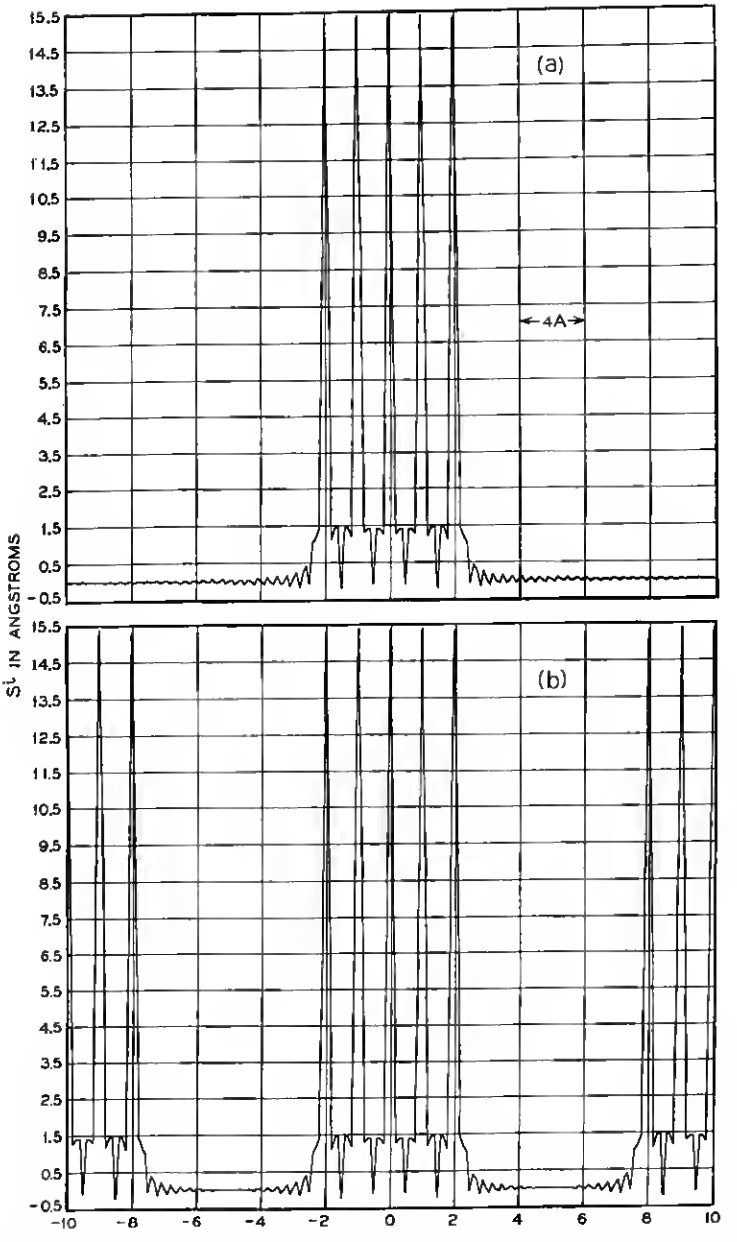

Fig. 8 — Computer-drawn image plane amplitude profiles aloug the axis x° of the nickel atom chain. For this case $a = 2$ Å, $n_1 = 5$ and $C_5' = \langle u_a^2 \rangle = 0$ in equation (12a). The sampling intervals in (a) are $\overline{\Delta\xi} = 0.01$ and $\Delta(x^\circ/a) = \Delta\eta = 0.1$. In (b) the sampling interval $\overline{\Delta\xi} = 0.1$ and the profile shows an aliasing period of $(\overline{\Delta\xi})^{-1} = 10$. The aliasing period in (a) is 100.

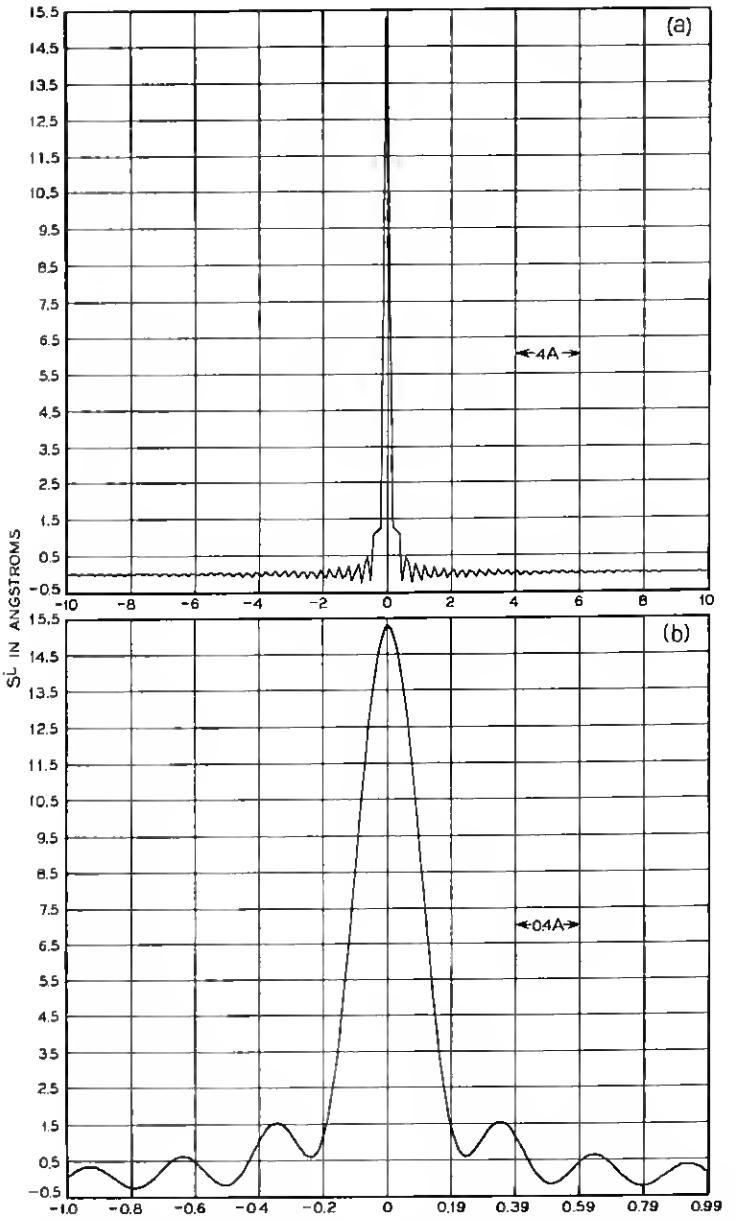

Fig. 9 — Profiles for equation (12) with $n_1 = 1$ nickel atom, $C_5' = 0$ and upper bounds $\xi_{max} = \eta_{max} = 2.5$ diffraction maxima; $\overline{\Delta\xi} = 0.01$ and $\Delta\eta = 0.1$. (a) Interval $\Delta(x/a) = 0.1$ resulting in unresolved structure near origin. (b) Interval $\Delta(x/a) = 0.01$ with expanded scale showing resolution of structure.

Fig. 10 — Effect of upper bound on ΔS^j: $n_1 = 1$ nickel atom and $C_{\bar{0}}' = 0$. The upper bound is 1.5 diffraction maxima and $\Delta(x/a) = \overline{\Delta\eta} = 0.1$ and $\overline{\Delta\xi} = 0.01$. Compare with Fig. 9.

with $\overline{\Delta\xi} = 0.01$, $\overline{\Delta\eta} = 0.1$ and $\Delta(x/a) = 0.1$. The profile is shown in Fig. 9(a). The number of points involved in this profile is

$$\frac{\eta_{\max}}{\overline{\Delta\eta}} \cdot \frac{\epsilon_{\max}}{\overline{\Delta\xi}} \cdot \frac{20}{\Delta\left(\frac{x}{a}\right)} = 25.4 \times 10^6.$$

The neighborhood of the central maximum shows irregularities that are smoothed out to a more faithful representation when $\Delta(x/a) = 0.01$ as seen in Fig. 9(b). The uumber of points involved in the profile is the same since the range has been reduced by a factor of ten.

The subsidiary maxima and minima near the principal maximum of Fig. 9(b) are due to aperture diffraction and would smooth out if the upper limit of tbe integral were extended to infinity. The radius of the atom in the profile is not distinct, since the shoulder of the maximum will approach the axis asymptotically.

Tbe size of the aperture given by the upper bounds $\xi_{\max}$ and $\eta_{\max}$ is reduced from 3.5 in Fig. 9(b) to 1.5 in Fig. 10. The reduction in aperture results in a loss of contrast to about 8 per cent. The upper bound 1.5 corresponds to an objective half-angle of 2.8×10^{-2} rad.

REFERENCES

1. Heidenreich, R. D., *Fundamentals of Transmission Electron Microscopy*. Interscience, New York, 1964; see Ch. V for elementary discussion.
2. *International Crystallographic Tables*, Vol. III, Kynoch Press, Birmingham, England, 1962.
3. Burge, R. E., and Smith, G. H., Proc. Phys. Soc., *79*, 1962, p. 673.
4. Williams, E. J., Proc. Roy. Soc., *A139*, 1933, p. 163.
5. Ref. 1, p. 308.

6. Ref. 1, Ch. X.
7. Ref. 1, p. 308.
8. Ref. 1, p. 107.
9. See Ref. 1, Ch. VIII for a detailed discussion of both the kinematic and dynamical theories.
10. Ref. 1 and also James, R. W., *Optical Principles of the Diffraction of X-Rays*, G. Bell and Sons, Ltd., London, 1954.
11. See Ref. 1, Appendix B.
12. Scherzer, O., J. Appl. Phys., *20*, 1949, p. 20.
13. Haine, M. E., *Electron Microscope*, Interscience, New York, 1961, p. 54.
14. See Ref. 1, p. 230.
15. Ref. 1, p. 140.
16. Ref. 1, p. 109.
17. For a discussion, see Hamming, R. W., *Numerical Methods for Scientists and Engineers*, McGraw-Hill, New York, 1962, p. 295.
18. See Ref. 1, p. 330.
19. See Ref. 1, p. 312.
20. Beer, M., J. Molecular Biology, *7*, 1963, p. 70.
21. Maradudin, A. A., Montroll, E. W., and Weiss, G. H., Solid-State Physics. *Advances in Research and Application*, Supp. 3, Academic Press, New York, 1963.
22. Horstmann, M., and Meyer, G., Phys. Kondens. Materie, *1*, 1963, p. 208.
23. Ref. 1, pp. 127 and 140.
24. Ref. 17, Ch. 8.
25. Ref. 17, p. 276.